INSTITUTE OF PHYSICS PUBLISHING NANOTECHNOLOGY
Nanotechnology **17** (2006) 2805–2812 doi:10.1088/0957-4484/17/11/013

Structural characterization and luminescence properties of nanostructured lanthanide-doped Sc_2O_3 prepared by propellant synthesis

R Krsmanović[1], O I Lebedev[1], A Speghini[2], M Bettinelli[2], S Polizzi[3] and G Van Tendeloo[1]

[1] EMAT, University of Antwerp, Groenenborgerlaan 171, B-2020 Antwerp, Belgium
[2] Dipartimento Scientifico e Tecnologico, Università di Verona and INSTM, UdR Verona, Strada le Grazie 15, 37134 Verona, Italy
[3] Dipartimento di Chimica Fisica, Università di Venezia and INSTM, UdR Venezia, Via Torino 155/b, 30172 Venezia, Mestre, Italy

E-mail: radenka.krsmanovic@ua.ac.be

Received 15 February 2006, in final form 3 April 2006
Published 16 May 2006
Online at stacks.iop.org/Nano/17/2805

Abstract
Nanocrystalline powders of undoped and lanthanide-doped scandium oxide were prepared by propellant synthesis and characterized by x-ray powder diffraction, electron microscopy, EDX spectroscopy and luminescence spectroscopy. The obtained material has the Sc_2O_3 cubic structure (space group $Ia\bar{3}$) with unit cell parameter increasing with the size of the dopant. The crystallite size is in the range 20–40 nm. The lanthanide-doped samples form $Sc_{2-x}Ln_xO_3$ solid solutions with $x \approx 0.2$ (Ln = Eu or Er). No inhomogeneity was found by microanalysis on the micron scale. The emission spectrum of the Eu^{3+} doped Sc_2O_3 sample shows strong bands in the visible region assigned to 4f–4f transitions of the lanthanide ions.

1. Introduction

Rare earth doped sequioxides yttria (Y_2O_3), lutetia (Lu_2O_3) and scandia (Sc_2O_3) have been found to be interesting materials for many technological applications in the field of optical devices, such as luminescent displays, optical amplifiers and solid state lasers [1–4]. Scandium oxide, in particular, has recently attracted the attention of many researchers for its interesting physical and chemical properties. Its high chemical stability, together with a high bulk refractive index value (1.90 at 400 nm) and a high ultraviolet cut-off (215 nm) [5], makes it interesting for numerous applications in the field of photonics and optoelectronics. Moreover, due to its high thermal conductivity, trivalent rare earth doped scandia is a very suitable host material for high power solid-state lasers [6]. The growth of a Sc_2O_3 single crystal by the conventional thermal heating–cooling method is difficult due to the extremely high melting temperature (2430 °C) [7]. On the other hand, efficient methods at lower temperature are employed to prepare Sc_2O_3 powders, such as an electrochemical method (at 950 °C) [8], a reverse-strike precipitation technique [9] and hydrothermal synthesis [10]. These methods provide crystalline materials with a high surface area.

On the other hand, the study of the luminescence properties of lanthanide doped nanocrystalline oxide particles has become of paramount importance, due to the fact that the optical and electronic properties of these nanocrystalline materials differ from those of the bulk samples and can be influenced by the particle size [11]. Many investigations have been carried out on lanthanide doped nanocrystalline Y_2O_3 and Lu_2O_3 [12, 13], but only a few papers have been published on rare earth doped nanocrystalline Sc_2O_3 [14, 15]. One of the recently employed preparation techniques of nanocrystalline materials is based on a combustion (propellant) synthesis. This technique is very useful for the preparation of rare earth doped luminescent materials in the form of nanocrystalline powders [15–18], and makes it possible to

optimize the parameters such as particle size and uniform distribution of activators, which influence the luminescence properties. Activators concentrated on the surface or on the grain boundaries are thought to be non-luminescent or quenching centres [19]. In particular for low voltage excitation, luminescent intensities are sensitive to the presence of contamination on the phosphor surface [20]. Hence, obtaining defect-free and surface-contaminant-free, homogeneously doped phosphor nanocrystals is very important.

In this paper, we show that scandium oxide in nanocrystalline form can be successfully obtained with the above-mentioned propellant technique. We investigated the structure and morphology of the synthesized powders, in particular the aggregation and particle size distribution, as well as the luminescence properties for the lanthanide-doped nanocrystalline scandia samples.

2. Experimental details

2.1. Synthesis

Nanocrystalline powders of Sc_2O_3 undoped and doped with 10 mol% of Eu^{3+} or Er^{3+}, $Sc_{1.8}Ln_{0.2}O_3$ (Ln = Eu or Er), were prepared using a propellant synthesis [21, 22]. An aqueous solution containing appropriate quantities of glycine (NH_2CH_2COOH) and metal nitrates, $Sc(NO_3)_3$ and $Ln(NO_3)_3$ (Ln = Er or Eu) was prepared starting from high purity (99.9%) reagents. The glycine serves as a fuel for the combustion reaction, being oxidized by the nitrate ions. A glycine-to-metal nitrate molar ratio of 1.2 was employed. The mixture was heated with a Bunsen flame until the solvent evaporated and auto-combustion occurred with the evolution of a brown fume. The synthesis reaction can be described by the following stoichiometric equation:

$$3M(NO_3)_3 + 5NH_2CH_2COOH + 9O_2 \rightarrow \tfrac{3}{2}M_2O_3 + \tfrac{5}{2}N_2\uparrow + 9NO_2\uparrow + 10CO_2\uparrow + \tfrac{25}{2}H_2O\uparrow$$

where M stands for Sc or the rare earth dopant (Eu or Er). After a few seconds, a porous voluminous powder was formed, occupying the entire volume of the reaction vessel.

The resultant powder of the combustion reaction was fired for 1 h at 500 °C in order to decompose any residual carbohydrazide and nitrate ions. All nanocrystalline samples were kept in air without any further precaution.

2.2. Structural investigation

The morphology, microstructure and local composition of the obtained scandia powders were studied by x-ray powder diffraction, electron microscopy and EDX analysis.

A Philips X'Pert vertical goniometer with Bragg–Brentano geometry, connected to a highly stabilized generator, was used for x-ray diffraction (XRD) measurements. Co Kα Fe-filtered radiation (λ = 1.788 97 Å), a graphite monochromator on the diffracted beam and a proportional counter with pulse height discriminator were used. The XRD data were collected at room temperature in the 2Θ (Bragg angle) range of 20°–100° with a step size of 0.05° and acquisition time of 10 s per point for three runs and then averaged. Diffraction data were analysed by fitting limited angular regions using previously described procedures [23, 24]: each peak is described by a couple of constrained pseudo-Voigt functions (Kα1 and Kα2 profiles) and the background by a polynomial function; parameters are optimized by the simplex method. In accordance with the Wagner method [25, 26], cell-edge values were extrapolated by applying a weighted least-square linear fit to the lattice parameter values calculated from the position of 20 reflections in the 2Θ range of 20°–86° as a function of $\cos\Theta\cot\Theta$. From the profile analysis of the XRD lines, average crystallite size and microstrains were determined by using the Warren–Averbach method [27, 28] on the 222/444 pairs of reflections. By using the Fourier coefficients of two different peaks from the same family of crystallographic planes, the distribution of crystallite dimensions and the corresponding distribution of microstrains $\langle\varepsilon^2(D)\rangle$ were obtained. Both distributions refer to the direction perpendicular to the (*hkl*) family of crystallographic planes. The value of the volume-weighted average crystallite size, $\langle D\rangle_v$, and the value of $\langle\varepsilon^2(D)\rangle$ at $\langle D\rangle_v/2$, taken as a measure of the average microstrains, were calculated. The instrumental broadening was previously deconvolved by using the Stokes's method adapted to analytically defined profiles [23, 24].

Scanning electron microscopy (SEM) observations were performed with a JEOL JEM-5510 equipped with an INCA x-ray microanalysis unit. The average composition of the samples was determined by x-ray energy dispersion (EDX) spectroscopy acquiring a spectrum for 600 s (live time) at an accelerating voltage of 30 kV. For this analysis, powders were cold-pressed into pellets of 3 mm diameter under a load of about 2 tons of pressure and then left uncoated.

Transmission electron microscopy (TEM) was used to obtain detailed information about the local structure and size distribution of the crystalline scandia nanoparticles. Electron diffraction and EDX analysis were carried out on a Philips CM20 microscope, equipped with a LINK-200, operating at 200 kV. High resolution electron microscopy (HREM) was performed on a JEOL 4000EX electron microscope (0.17 nm point resolution) operating at 400 kV. TEM specimens were prepared by ultrasonically dispersing the finely crushed powdered sample in ethanol and depositing drops of this suspension on a holey carbon film grid. The CrystalKitX and MacTempas software packages were used to simulate HREM images and electron diffraction patterns.

2.3. Spectroscopic characterization

The 488.0 nm line of an argon laser was used to excite the luminescence spectra. A fibre optic probe was employed to collect the emission signal. The scattered signal was analysed using a half-meter monochromator equipped with a CCD detector. A 1200 lines mm^{-1} grating was used to collect the luminescence spectrum in the region of the $^5D_0 \rightarrow {}^7F_0$ transition of the Eu^{3+} ion (578–583 nm, resolution of about 0.02 nm), whilst the laser-excited luminescence spectrum in the wider 500–700 nm range was measured using a 150 lines mm^{-1} grating (resolution of about 0.15 nm). All the spectroscopic measurements were performed at room temperature.

The Eu^{3+} ion emission decay curve was measured using the second harmonic radiation (532.0 nm) of a Nd–YAG pulsed laser as the excitation source. The scattered

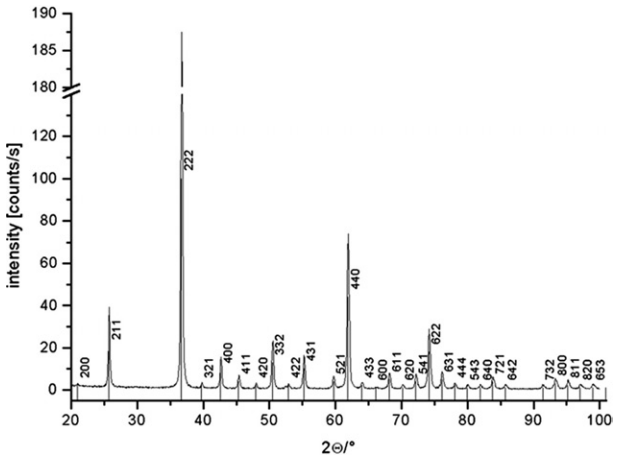

Figure 1. XRD pattern for the undoped nanocrystalline Sc_2O_3 sample. Lines denote the peak positions of Bragg reflections.

Table 1. Unit cell lattice parameter a, and crystallite dimensions $\langle D\rangle_v$ for Sc_2O_3, Sc_2O_3:Er^{3+} and Sc_2O_3:Eu^{3+} samples are obtained from XRD data, whereas D-values of average particle size (with standard deviation) are measured from TEM images for about 150 particles.

Sample	a (Å)	$\langle D\rangle_v$ (nm) 222/444	D (nm)	Ionic radius (Å) [36]
Sc_2O_3	9.8378(7) [15]	37 [15]	40 ± 4	Sc^{3+}—0.745
Sc_2O_3:Er^{3+}	9.9056(5) [15]	27 [15]	37 ± 3	Er^{3+}—0.890
Sc_2O_3:Eu^{3+}	9.9170(1)	14	22 ± 2	Eu^{3+}—0.947

signal was analysed using a half-meter monochromator (with 150 lines mm^{-1} grating) and detected with a GaAs water cooled photomultiplier and stored in a 500 MHz digital oscilloscope.

3. Results and discussion

3.1. X-ray diffraction

The x-ray powder diffraction pattern of the obtained undoped nanocrystalline scandium oxide is shown in figure 1. The XRD spectrum can be matched by a single-phase cubic structure (space group $Ia\bar{3}$) with cell parameter $a = 9.8378(7)$ Å [15]. The cell parameter is slightly smaller than the value given in the reference file for the bulk Sc_2O_3 (9.8450(4) Å) [29]. This phenomenon of lattice contraction has been noticed for nanostructured materials and explained as a consequence of the large surface tension due to the increased surface-to-volume ratio [30, 31]. For the Sc_2O_3:Eu^{3+} and Sc_2O_3:Er^{3+} doped samples a small shift of the position of the diffraction peaks towards lower 2Θ values is observed, which indicates slightly larger unit cells, consistent with the larger size of the dopant cations with respect to the host Sc^{3+} cations. The unit cell parameters obtained from XRD measurements and their dependence on the dopant radii are shown in table 1.

Estimated values for the mean crystallite size are calculated from the diffraction peak width of 222/444 pairs of reflections (table 1). It has been found that the crystallite size decreases with increasing the dimension of the dopant cation: from 37 nm for Sc_2O_3 and 27 nm for Sc_2O_3:Er^{3+} (as previously reported in [15]) to a minimum value of 14 nm for Sc_2O_3:Eu^{3+}. The same behaviour was observed on garnets produced with propellant synthesis [16, 21]. For all samples the calculated values of $\langle \varepsilon^2(D)\rangle$ at $\langle D\rangle_v/2$ are very small, so we presume that no significant microstrains are present.

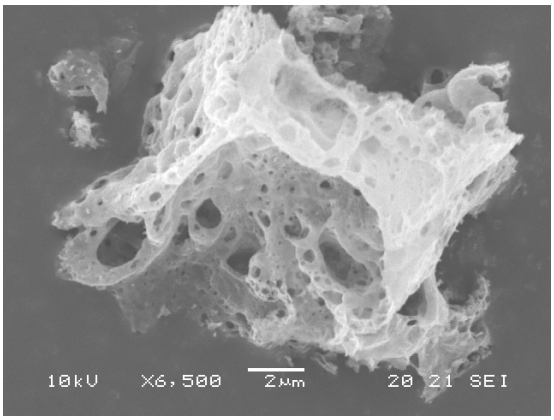

Figure 2. SEM image of the Sc_2O_3 sample.

3.2. Electron microscopy

SEM observations of scandia samples show agglomerates ranging from a few microns to a few tens of microns with a highly porous, sponge-like morphology (figure 2), typical for samples prepared with the propellant technique [16, 21, 32]. The spectra obtained from EDX analyses in SEM (figure 3) qualitatively confirm the presence of the lanthanide dopants. A quantitative EDX analysis shows that the average elemental ratios (with standard deviation in brackets) Sc/Eu = 10.15(0.12) and Sc/Er = 9.89(0.15) are close to those expected from a solid solution of composition $Sc_{1.8}Ln_{0.2}O_3$ (Ln = Eu, Er). The homogeneity of the samples on a micrometre scale is checked using an EDX mapping technique. Elemental maps of Sc, O, Eu and Er show a uniform density distribution (maps not shown), confirming that the distribution of europium and erbium is homogeneous throughout the material.

TEM images show highly agglomerated crystalline nanoparticles with an irregular, polygonal-like, sharp-edge shape and variable dimensions (figure 4). These particles are single crystallites that make up the walls of the porous structure observed by SEM (figure 2). The agglomeration of nanoparticles is usually explained as a common way to minimize their surface free energy [31, 33]. However, in some works the agglomeration is assigned to the presence of organic residuals that act as 'binders' for the crystallites [34, 35]. Since we did not observe in the IR spectra (not shown) any vibration bands due to organic residuals, around 3000 cm^{-1}, this option is excluded. The small voids present within some particles (see for example the two arrows in figure 4(a)) are generated by the large amount of gas produced during the rapid combustion synthesis reaction. Their presence usually tend to yield under-estimated values of the crystallite sizes obtained from the XRD broadening analysis (table 1), since a void interrupts the diffraction coherence of this crystallite. In the present samples this effect is not very large (see table 1),

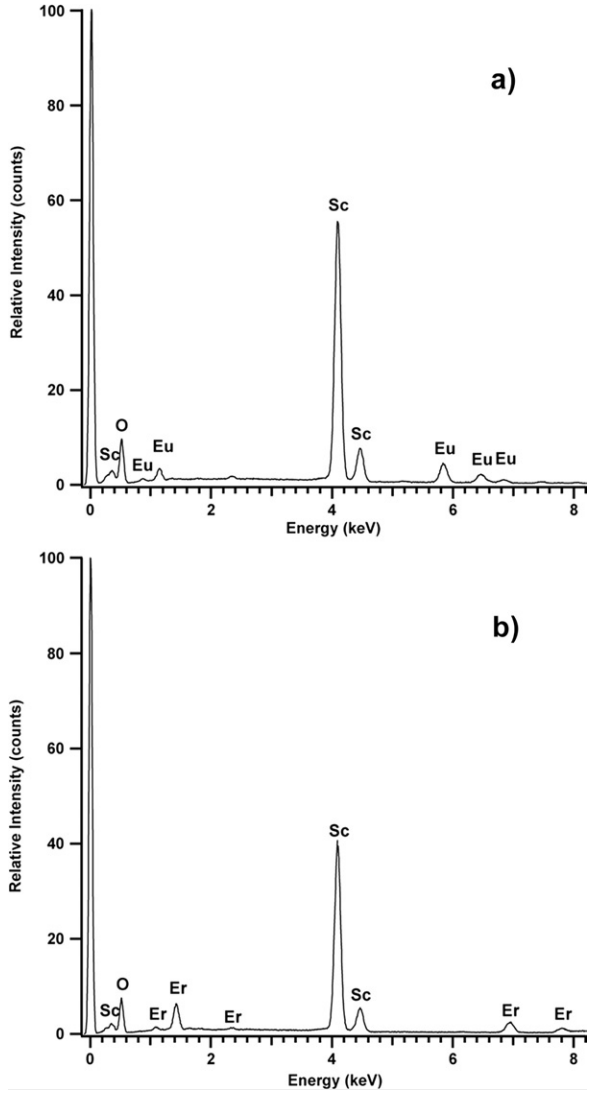

Figure 3. EDX spectra for doped scandia samples: (a) Sc_2O_3:Eu^{3+} and (b) Sc_2O_3:Er^{3+}.

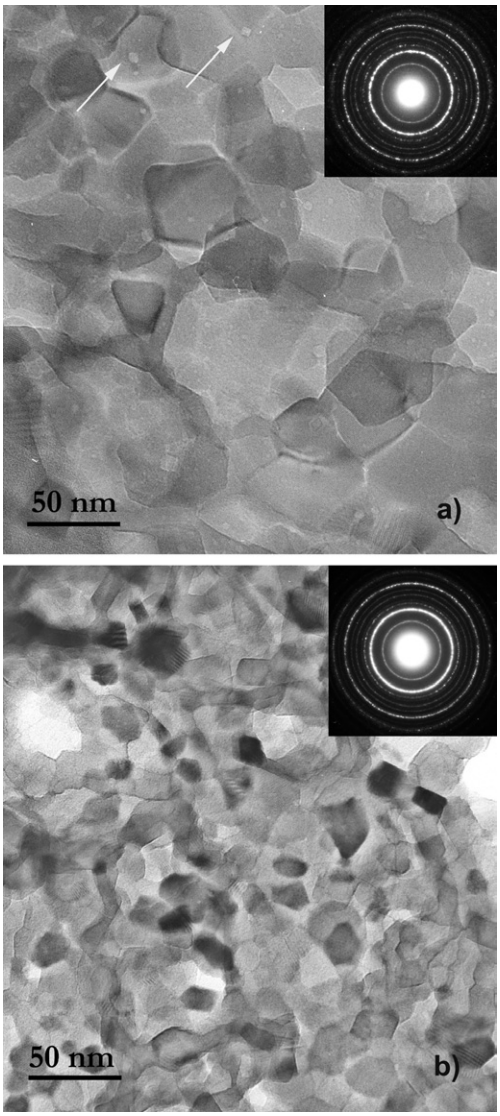

Figure 4. TEM images and corresponding ED patterns of (a) Sc_2O_3 and (b) Sc_2O_3:Eu^{3+}.

considering that an error of 10–15% is usually associated with XRD determinations: the average particle size determined from TEM observations for Sc_2O_3 and Sc_2O_3:Er^{3+} is about 40 nm, whereas for Sc_2O_3:Eu^{3+} almost half of this value was found. The particle size distributions have been determined by measuring the maximum dimension of 123 particles for both Sc_2O_3 and Sc_2O_3:Er^{3+}, and 165 particles for the Sc_2O_3:Eu^{3+} sample. This is illustrated with appropriate histograms in figure 5.

The local crystal structure was investigated by electron diffraction (ED) and high resolution TEM. The single phase Sc_2O_3 was confirmed for all three samples, by analysing the electron diffraction rings. The sharp rings (see insets in figures 4(a) and (b)) arise from the fine grain size of the polycrystalline material and the fact that the ED patterns are taken over a region of about 1 μm. In figure 6 the ED patterns of Sc_2O_3 and Sc_2O_3:Eu^{3+} are compared. The lattice parameters calculated from the ED patterns and the difference between them are in good agreement with the values determined from x-ray powder diffraction data.

The internal structure and the quality of the scandia nanocrystals have been investigated by HREM. Figure 7(a) shows part of a Sc_2O_3 nanocrystal viewed along the [011] zone axis, where the bright dots in the HREM image correspond to the Sc atom columns. The computer simulation, given as an inset and based on cubic scandia with space group $Ia\bar{3}$, matches well the experimental image. The surface of observed nanocrystals is free of defects and without any amorphous layer. Also, for the doped scandia samples, we observed a well crystalline structure of Sc_2O_3 without any irregularities or local cation ordering in grain boundaries. Figure 7(b) shows a grain of Sc_2O_3:Eu^{3+} in contact with neighbouring grains.

EDX analyses in the TEM show a homogeneous lanthanide-ion doping, even at a local nanometre scale. Quantitative EDX analysis shows a slightly different ratio in average elemental concentrations: $Sc/Eu \approx 9.0 \pm 0.6$, $Sc/Er \approx 8.0 \pm 0.4$ (the stoichiometric ratio is 9). The results of this quantitative EDX analysis, performed on approximately 25 different crystallites, are presented in table 2, with the average

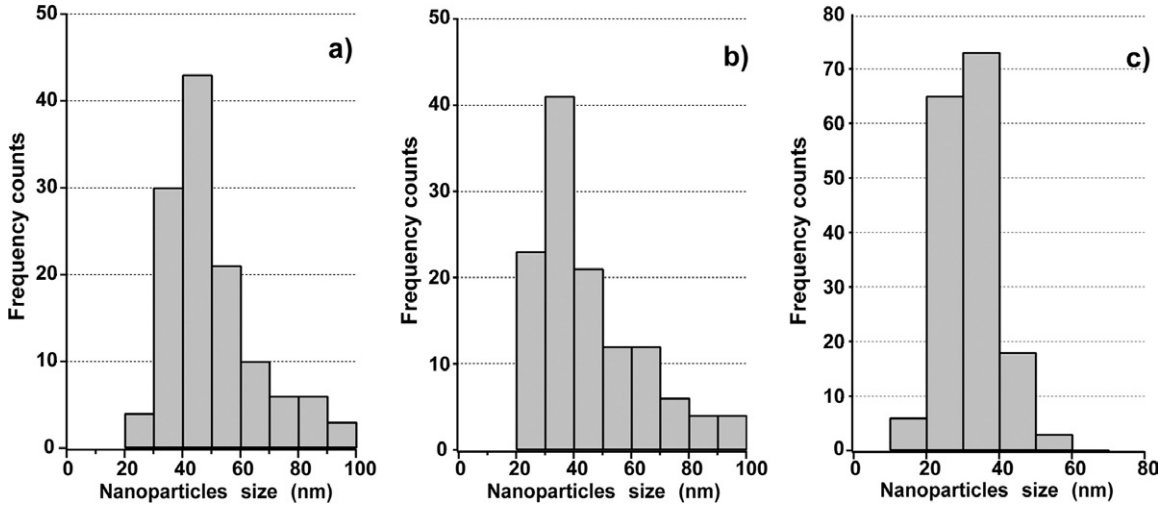

Figure 5. Nanoparticle size distribution for (a) Sc_2O_3, (b) Sc_2O_3:Er^{3+} and Sc_2O_3:Eu^{3+}.

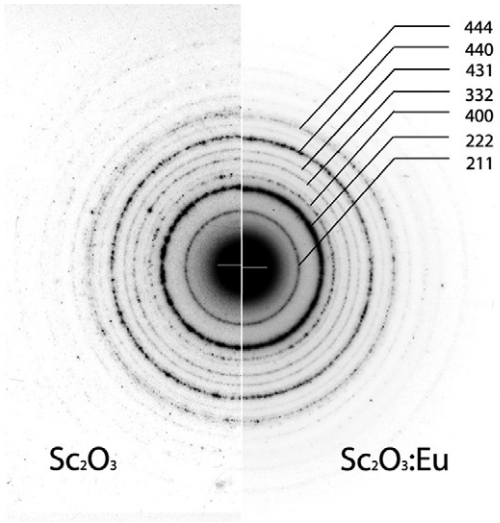

Figure 6. Electron diffraction patterns of Sc_2O_3 and Sc_2O_3:Eu^{3+} with indexed rings.

values for stoichiometry and relevant standard deviations. During the experiment the diameter of the analysing spot has been varied in correspondence with the diameter of the observed nanocrystals. HREM as well as EDX confirm that lanthanide-doped scandia samples are homogeneous, with good crystal quality and with the required stoichiometry $Sc_{2-x}Ln_xO_3$ ($x \approx 0.2$) (Ln = Eu or Er). These results and results from XRD analysis show that the propellant synthesis produces a very good solid solution of cubic, nanocrystalline scandia.

3.3. Luminescence

The cubic Sc_2O_3 lattice can accommodate the Eu^{3+} dopant ion in two distinct sites, which have point-group symmetry C_2 and C_{3i}. The relative abundance of the two C_2 and C_{3i} sites in the crystal structure is 3:1, respectively [15]. According to the transition selection rules, the electric dipole transitions for the Eu^{3+} ions occupying the C_2 sites are allowed, while

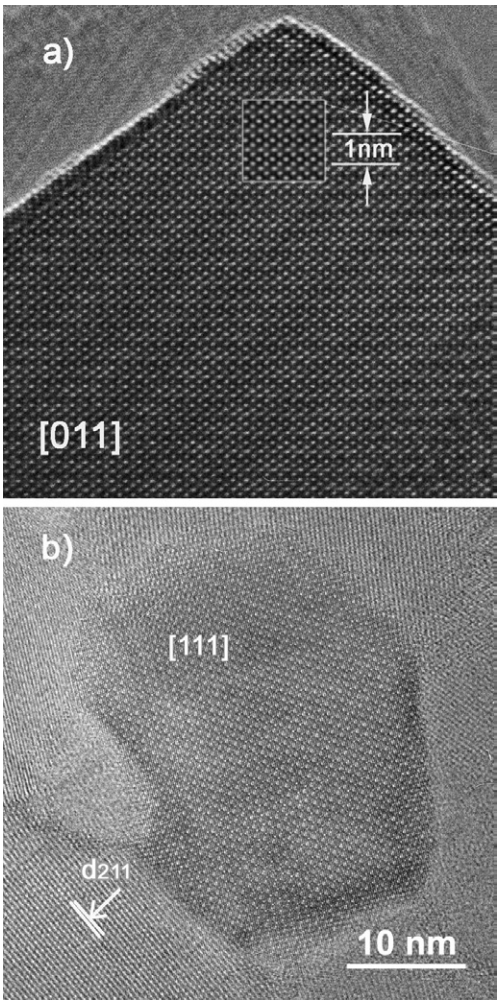

Figure 7. HREM images of (a) Sc_2O_3 along the [011] zone with the simulated image (as inset) for a defocus of −70 nm and a thickness of 13 nm; (b) one grain of Sc_2O_3:Eu^{3+}; grain boundaries are well defined, no amorphous layer or irregularities observed.

those for the Eu^{3+} ions in the C_{3i} sites are forbidden. On the other hand, for the Eu^{3+} ions in the C_{3i} site only magnetic

Table 2. Results of EDX quantitative analysis in the TEM for 25 particles of Sc_2O_3:Eu^{3+} and Sc_2O_3:Er^{3+} samples. R is the cation (at.%) ratio Sc/Ln (Ln = Eu or Er).

Sample	Sc K (at.%)	Eu L (at.%)	Er L (at.%)	R	x (at.%)
$Sc_{2-x}Eu_xO_3$	90.0 ± 0.6	10.0 ± 0.6	—	9.0 ± 0.6	0.20 ± 0.01
$Sc_{2-x}Er_xO_3$	88.9 ± 0.5	—	11.1 ± 0.5	8.0 ± 0.4	0.18 ± 0.01

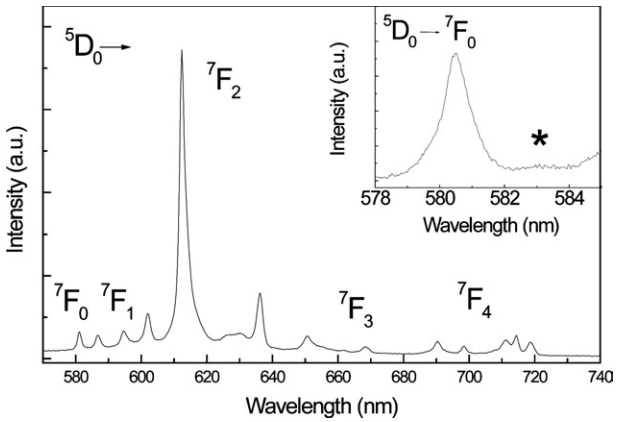

Figure 8. Room temperature emission spectra for the nanocrystalline Sc_2O_3:Eu^{3+} sample ($\lambda_{exc} = 488.0$ nm). The * symbol in the inset indicates the extremely weak $^5D_0 \rightarrow {}^7F_{1a}$ magnetic dipole transition of Eu^{3+} ions in sites of C_{3i} symmetry [37].

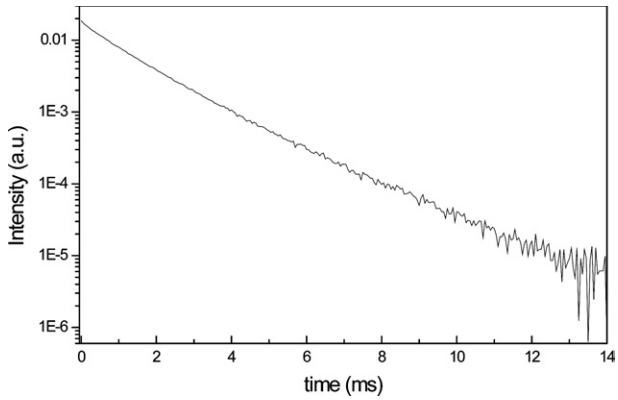

Figure 9. Room temperature emission decay curve for the nanocrystalline Sc_2O_3:Eu^{3+} sample ($\lambda_{exc} = 532$ nm, $\lambda_{em} = 612$ nm).

dipole transitions should be observed. The room temperature laser-excited luminescence spectra of the $Sc_{1.8}Eu_{0.2}O_3$ sample measured with an excitation wavelength of 488.0 nm are shown in figure 8. The wider spectrum in the 570–740 nm range shows 4f → 4f emission bands assigned to transitions from the $^5D_0$ excited state to the ^7F_J ($J = 0, 1, 2, 3, 4$) lower lying multiplets of the Eu^{3+} ion. In particular, the strongest band in the spectrum is observed at 612 nm and it is assigned to transitions between the $^5D_0$ and the lower lying $^7F_2$ levels of the Eu^{3+} ion in sites of C_2 symmetry. Moreover, the three weak emission bands located at 587, 595 and 602 nm are assigned to transitions between the $^5D_0$ level and the three $^7F_1$ Stark levels of the Eu^{3+} ion in sites of C_2 symmetry [37, 38]. Besides, the emission band at 580.5 nm observed for the $^5D_0 \rightarrow {}^7F_0$ transition is attributed to Eu^{3+} ions in sites of C_2 symmetry [37] (see the inset of figure 8). On the basis of symmetry arguments, two magnetic dipole $^5D_0 \rightarrow {}^7F_1$ transitions are expected in the luminescence spectrum, as the $^7F_1$ multiple of the Eu^{3+} ion in a site of C_{3i} site symmetry split in two energy levels. The extremely weak band located at about 583 nm (see the inset of figure 8) can be identified as the $^5D_0 \rightarrow {}^7F_{1a}$ magnetic dipole transition of Eu^{3+} ions in sites of C_{3i} symmetry, following the assignments proposed by Malta *et al* [37]. The luminescence band due to the second $^5D_0 \rightarrow {}^7F_{1b}$ magnetic dipole transition is most probably superimposed on the stronger bands due to the $^5D_0 \rightarrow {}^7F_1$ transitions of Eu^{3+} ions in sites of C_2 symmetry, making its identification and assignment difficult in the present experimental conditions. In general, the peak positions of the emission bands are very similar to those observed for Eu^{3+} doped Sc_2O_3 polycrystalline (bulk) samples [37, 38]. It is worth noting that the probability of the magnetic dipole $^5D_0 \rightarrow {}^7F_1$ transition is practically independent of the local environment around the lanthanide ion. On the other hand, the $^5D_0 \rightarrow {}^7F_2$ transition is purely of electric dipole nature and it is very sensitive to the environment of the lanthanide ion; for this reason it is called a hypersensitive transition. In particular, the integrated emission intensity of the $^5D_0 \rightarrow {}^7F_2$ transition depends strongly on the site symmetry of the Eu^{3+} ion, differently from that of the $^5D_0 \rightarrow {}^7F_1$ transition, which does not. For this reason the asymmetry ratio

$$R = \frac{I(^5D_0 \rightarrow {}^7F_2)}{I(^5D_0 \rightarrow {}^7F_1)} \tag{1}$$

of the integrated intensities of the $^5D_0 \rightarrow {}^7F_2$ and $^5D_0 \rightarrow {}^7F_1$ transitions is indicative of the asymmetry of the coordination polyhedron of the Eu^{3+} ion [39, 40]. In particular, the lower the R value, the higher the site symmetry of the Eu^{3+} ion. The obtained R value for the nanocrystalline scandia under investigation is 5.3 ± 0.1. The high asymmetry ratio value indicates that the local environment of the Eu^{3+} ion is notably distorted, in agreement with a C_2 symmetry for the sites mainly occupied by the dopant ions.

The luminescence decay curve measured at 612 nm after excitation at 532 nm for the nanocrystalline Eu^{3+} doped Sc_2O_3 sample is shown in figure 9. As can be clearly seen from the figure, the decay curve is not exponential. For this reason, we calculated the effective emission decay time τ_{eff} using equation [41]:

$$\tau_{eff} = \frac{\int t I(t) \mathrm{d}t}{\int I(t) \mathrm{d}t} \tag{2}$$

where $I(t)$ represents the luminescence intensity at time t corrected for the background and the integrals are evaluated on a range $0 < t < t_m$ where $t_m \gg \tau_{eff}$. The obtained τ_{eff} value for the nanocrystalline samples is 1.49 ± 0.05 ms. The

non-exponential behaviour of the luminescence decay curves could be due to several effects, such as the disorder affecting the Eu^{3+} sites, energy transfer (ET) processes among the Eu^{3+} ions or the size distribution of the nanoparticles. Moreover, it would be reasonable to expect a shortening of the Eu^{3+} emission decay time for the present highly doped Eu^{3+} scandia with respect to less concentrated Eu^{3+} scandia samples, due to some energy transfer processes between the Eu^{3+} ions (concentration quenching of the luminescence).

The average ion distance in a crystalline host can be estimated from equation [42]:

$$d = \left(\frac{3}{4\pi N}\right)^{1/3} \tag{3}$$

where N is the ion density (ion $Å^{-3}$). Considering the unit cell parameter for the Eu^{3+} doped Sc_2O_3 nanocrystalline sample (see table 1) the unit cell volume turns out to be 975.31 $Å^3$, slightly larger than that obtained for an Er^{3+} doped Sc_2O_3 nanocrystalline sample [15]. This behaviour is compatible with the higher ion radius of the Eu^{3+} ion with respect to the Er^{3+} one. Taking into account the Eu^{3+} concentration in the scandia host under investigation, the Eu^{3+}–Eu^{3+} average distance calculated from equation (3) turns out to be 4.17 Å, similar to the value found for an Er^{3+} doped Sc_2O_3 nanocrystalline sample [15]. Moreover, it can be noted from table 1 that the average particle size for the Eu^{3+} doped nanocrystalline scandia is 22 nm. Considering a spherical nanoparticle of such dimensions, the average number of luminescent lanthanide ions in this nanoparticle is estimated to be about 20.

Nonetheless, the $^5D_0$ effective decay time of the Eu^{3+} ion observed for the nanocrystalline scandia under investigation appears to be significantly longer than for more diluted (∼2 at.%) Eu^{3+} doped bulk cubic Sc_2O_3 ($\tau = 0.8$ ms) [43]. The lengthening of the emission decay times for Eu^{3+} doped nanocrystalline oxide hosts with respect to the corresponding micrometre size (bulk) samples has been already observed for Eu^{3+} doped nanocrystalline Y_2O_3 [44], Lu_2O_3 [45] and ZrO_2 [46]. This behaviour can be explained considering that the effective refractive index (n_{eff}) surrounding the Eu^{3+} ion in the porous nanocrystalline material is lower with respect to the micrometre size host [44]. This explanation is compatible with the nanometre particle size of the host (see TEM micrographs, figures 4 and 7, and particle size distribution, figure 5). In fact, for these structural characteristics it is reasonable that the filling factor (the fraction of the volume of the host occupied by the nanoparticles) is lower than one.

4. Conclusions

This paper shows that pure and lanthanide doped nanocrystalline scandia can be obtained by a propellant synthesis. The structure is confirmed to be cubic (space group $Ia\bar{3}$) with a slightly smaller cell parameter than in the bulk material ($a =$ 9.8378(7) Å). XRD analysis of doped samples shows only one phase, cubic scandia, despite the heavy doping of the Sc_2O_3 matrix. The cell parameters change with lanthanide doping as expected from the larger dopant cations: Sc_2O_3:Er^{3+} ($a =$ 9.9056(5) Å) and Sc_2O_3:Eu^{3+} ($a =$ 9.9170(1) Å). Electron microscopy shows that powder agglomerates of scandia samples are constituted of aggregated single crystal particles with an irregular, polygonal sharp-edge shape and a major size distribution ranging from 20 to 40 nm. Electron diffraction confirmed the presence of a single phase Sc_2O_3 at the local level. HREM, for pure and doped samples, showed a well-ordered structure of Sc_2O_3 crystals without any defects or local ordering of lanthanide ions. EDX microanalyses confirm that lanthanide dopants are homogeneously distributed. Results of quantitative EDX analysis demonstrate that a solid solution with stoichiometry $Sc_{2-x}Ln_xO_3$ has effectively been obtained within the composition range $0.19 < x < 0.21$ in the case of Sc_2O_3:Eu^{3+} and $0.17 < x < 0.19$ for Sc_2O_3:Er^{3+}. The laser excited luminescence spectra of the Eu^{3+} doped Sc_2O_3 sample show strong bands in the visible region assigned to $^5D_0 \rightarrow {}^7F_J$ ($J = 0, 1, 2, 3, 4$) transitions. The presence of a narrow peak at 612 nm, similar to that found for Eu^{3+} doped Y_2O_3, and a long luminescence lifetime at room temperature, suggest that the present nanocrystalline material can be used as a red phosphor in optoelectronic devices, such as luminescent displays. On the other hand, it should be remarked that the present Eu^{3+} doped material is most probably not well suited for applications which require fast luminescent responses.

Acknowledgments

This work has been performed within the framework of the Belgian IAP5-01 project and the 2003 PRIN/Cofin contract of the Italian Ministry for University and Research (MURST). Mr Tiziano Finotto is acknowledged for the XRD experimental work and Mrs Erica Viviani for technical assistance in the preparative work.

References

[1] Blasse G and Grabmeier B C 1994 *Luminescent Material* (Berlin: Springer)
[2] Ronda C R 1997 *J. Lumin.* **72** 49
[3] Brenier A and Boulon G 2001 *Europhys. Lett.* **55** 647
[4] Pradhan A K, Zhang K, Mohanty S, Dadson J, Hunter D, Loutts G B, Roy U N, Cui Y, Burger A and Wilkerson A L 2005 *J. Appl. Phys.* **97** 023513
[5] Horowitz C T and Gschneidner G A 1975 *Scandium* (New York: Academic)
[6] Peters V, Mix E, Fornasiero L, Petermann K, Huber G and Basun S A 2000 *Laser Phys.* **10** 417
[7] Petermann K, Fornasiero L, Mix E and Peters V 2002 *Opt. Mater.* **19** 67
[8] Masui T, Kim Y W, Imanaka N and Adachi G 2004 *J. Alloys Compounds* **374** 97
[9] Fokema M D and Ying J Y 1998 *Appl. Catal.* B **18** 71
[10] Zhang Y W, Liu J H, Si R, Yan Z G and Yan C H 2005 *J. Phys. Chem.* B **109** 18234
[11] Tissue B M 1998 *Chem. Mater.* **10** 2837
[12] Wakefield G, Holland E, Dobson P J and Hutchison J L 2001 *Adv. Mater.* **13** 1557
[13] Strek W, Zych E and Hreniak D 2002 *J. Alloys Compounds* **344** 332
[14] Xu G, Zhang Y W, Liao C S and Yan C H 2004 *J. Am. Ceram. Soc.* **87** 2275
[15] Vetrone F, Boyer J C, Capobianco J, Speghini A, Bettinelli M, Krsmanovic R and Polizzi S 2005 *J. Electrochem. Soc.* **152** 19
[16] Krsmanovic R, Polizzi S and Canton P 2005 *Mater. Sci. Forum* **494** 143

[17] Francini R, Pietrantoni S, Zambelli M, Speghini A and Bettinelli M 2004 *J. Alloys Compounds* **380** 34
[18] Boyer J C, Vetrone F, Capobianco J A, Speghini A and Bettinelli M 2004 *J. Phys. Chem.* B **108** 20137
[19] McKittrik J, Shea L E, Bacalski C F and Bosze E J 1999 *Displays* **19** 169
[20] Yoo J S and Lee J D 1997 *J. Appl. Phys.* **81** 2810
[21] Krsmanovic R, Canton P, Speghini A, Bettinelli M and Polizzi S 2004 *Mater. Sci. Forum* **453/454** 251
[22] Tessari G, Bettinelli M, Speghini A, Ajò D, Pozza G, Depero L E, Allieri B and Sangaletti L 1999 *Appl. Surf. Sci.* **144/145** 686
[23] Enzo S, Polizzi S and Benedetti A 1985 *Z. Kristallogr.* **170** 275
[24] Enzo S, Fagherazzi G, Benedetti A and Polizzi S 1988 *J. Appl. Crystallogr.* **21** 536
[25] Wagner N J 1966 *Met. Soc. Conf.* vol 36, ed J B Cohen (New York: Gordon and Breach)
[26] Adler R P I and Wagner C N J 1962 *J. Appl. Phys.* **33** 3451
[27] Warren B E and Averbach B L 1950 *J. Appl. Phys.* **21** 595
[28] Warren B E and Averbach B L 1952 *J. Appl. Phys.* **23** 497
[29] *Powder Diffraction File* JCPDS International Centre for Diffraction Data, Swarthmore PA, PDF n.42-1463
[30] Hofmeister H, Tan G L and Dubiel M 2005 *J. Mater. Res.* **20** 1551
[31] Li Q, Gao L and Yan D 1997 *Nanostruct. Mater.* **8** 825
[32] Fagherazzi G, Polizzi S, Bettinelli M and Speghini A 2000 *J. Mater. Res.* **15** 586
[33] Eilers H 2006 *Mater. Lett.* **60** 214
[34] Veith M, Mathur S, Kareiva A, Jilavi M, Zimmer M and Huch V 1999 *J. Mater. Chem.* **9** 3069
[35] Muliuoliene I, Mathur S, Jasaitis D, Shen H, Sivakov V, Rapalaviciute R, Beganskiene A and Kareiva A 2003 *Opt. Mater.* **22** 241
[36] Lide D R (ed) 1998 *Handbook of Physics and Chemistry* (Boca Raton, FL: CRC Press)
[37] Malta O L, Antic-Fidancev E, Lemaitre-Blaise M, Mililic-Tang A and Taibi M 1995 *J. Alloys Compounds* **228** 41
[38] Antic-Fidancev E, Holsa J and Lastusaari M 2002 *J. Alloys Compounds* **341** 82
[39] Oomen E W J L and van Dongen A M A 1989 *J. Non-Cryst. Solids* **111** 205
[40] Reisfeld R, Zigansky E and Gaft M 2004 *Mol. Phys.* **102** 1319
[41] Nakazawa E 1999 *Phosphor Handbook* ed S Shionoya and W M Yen (Boca Raton, FL: CRC Press) p 104
[42] de Sousa D F, Batalioto F, Bell M J V, Oliveira S L and Nunes L A O 2001 *J. Appl. Phys.* **90** 3308
[43] West G A and Clemens N S 1992 *J. Lumin.* **54** 245
[44] Meltzer R S, Feofilov S P, Tissue B and Yuan H B 1999 *Phys. Rev.* B **60** R14012
[45] Boyer J C, Vetrone F, Capobianco J A, Speghini A and Bettinelli M 2004 *J. Phys. Chem.* B **108** 20137
[46] Speghini A, Bettinelli M, Riello P, Bucella S and Benedetti A 2005 *J. Mater. Res.* **20** 2780